PHYSICAL REVIEW D

PARTICLES, FIELDS, GRAVITATION, AND COSMOLOGY

THIRD SERIES, VOLUME 46, NUMBER 10 15 NOVEMBER 1992

## RAPID COMMUNICATIONS

*Rapid Communications are intended for important new results which deserve accelerated publication, and are therefore given priority in editorial processing and production. A Rapid Communication in* **Physical Review D** *should be no longer than five printed pages and must be accompanied by an abstract. Page proofs are sent to authors, but because of the accelerated schedule, publication is generally not delayed for receipt of corrections unless requested by the author.*

# Trapping a geon: Black hole formation by an imploding gravitational wave

Andrew M. Abrahams*
*Center for Radiophysics and Space Research, Cornell University, Ithaca, New York 14853*

Charles R. Evans
*Department of Physics and Astronomy, University of North Carolina, Chapel Hill, North Carolina 27599*
(Received 9 June 1992)

We describe the formation of a black hole via the implosion of an axisymmetric gravitational wave. Finite difference simulations of the vacuum Einstein equations are used to obtain these results. The initial data consist of nearly linear solutions to the vacuum constraint equations that represent even-parity, ingoing wave packets with quadrupole angular dependence. A black hole is demonstrated to form as a result of imploding a wave packet with a sufficiently large value of a strength parameter, $\Theta \equiv 2\pi M_p/\lambda = 1.06 > \Theta_{\rm crit} \simeq 0.80$, where $2\lambda$ is the radial width of the wave packet and $M_p$ denotes its mass. Black hole formation is verified by observing (i) the exponential collapse of the central value of the lapse function $\alpha$, (ii) the formation of a trapped region and marginally outer-trapped surfaces, and (iii) the emission of quasi-normal-mode radiation. For the $\Theta = 1.06$ case, just over 2% of the mass emerges in normal-mode radiation.

PACS number(s): 04.30.+x, 04.20.Jb, 97.60.Lf

Recently, Beig and Ó Murchadha [1] have proven that it is possible to construct (nonsingular) sequences of time-symmetric, vacuum, asymptotically flat initial data that contain outer-trapped surfaces as they approach the strong-field limit of general relativity. Although a theorem of Penrose [2] can be invoked to show that the evolution of this initial data will lead to a singularity, it has not yet been shown that this singularity will be contained within the region of trapped surfaces. In a related effort [3], one-parameter sequences of time-symmetric initial data have been numerically constructed. Some of these sequences become singular inside a region of trapped surfaces, while others represent highly prolate wave packets that can be made arbitrarily singular without the appearance of outer-trapped surfaces.

In this paper, we use a *dynamical* calculation to follow the formation of a black hole as a gravitational wave implodes, gravitationally traps itself (forming a "geon" [4]), and collapses. Simulations of this type have also been performed by Miyama [5] and Stark [6]. The gravitational wave is initialized as ingoing, quadrupole radiation confined to a wave packet that has a narrow radial extent and a spherical wave front. It is important to note that although the wave front is initially spherical, the quadrupole angular dependence ensures that the gravitational field is nonspherical. Such wave packets undoubtedly lack the generality required to test the validity of cosmic censorship. These calculations do, however, add to the very small set of spacetimes known to form horizons following the evolution of highly asymmetrical fields and matter [6,7]. They also demonstrate the ability to detect the presence of trapped regions and locate marginally

*Also at Center for Theory and Simulation in Science and Engineering, Cornell University.

 

outer-trapped surfaces (MOTS's), to calculate gravitational radiation, and to read off wave forms at finite radius. All of these are techniques required to further investigate cosmic censorship. Extremely prolate wave packets [3] may be interesting vacuum analogues of the prolate collisionless-matter spheroids studied in Ref. [7].

Simulations were computed using an axisymmetric numerical relativity code [8] specialized to $T^{\mu\nu}=0$. This finite-difference code has been extensively tested and used to compute nonrotating gravitational collapse [9,10], oscillations of relativistic stars [11], and head-on collisions of compact stars [12]. More details about this code can be found in Ref. [9].

The code employs the quasi-isotropic spatial gauge, the analytic properties of which have been explored in Refs. [8,9,13,14]. In this gauge, assuming axisymmetry and no rotation, the 3+1 form of the line element in spherical-polar coordinates is

$$ds^2=-\alpha^2dt^2+\phi^4[e^{2\eta/3}(dr+\beta^r dt)^2 +r^2e^{2\eta/3}(d\theta+\beta^\theta dt)^2 +e^{-4\eta/3}r^2\sin^2\theta\, d\varphi^2]\ , \quad (1)$$

where $\alpha$ is the lapse function, $\beta^r$ and $\beta^\theta$ are shift vector components, $\phi$ is the conformal factor, and $\eta$ is the even-parity "radiative" variable. The extrinsic curvature $K^i{}_j$ and other tensors are projected on coordinate bases.

The maximal slicing condition $K^i{}_i=0$ results in an elliptic equation for $\alpha$. Components $\beta^r$ and $\beta^\theta$ are related by a first-order elliptic system, which arises to maintain the quasi-isotropic form of the line element. For these vacuum models a partially constrained evolution scheme is used, in which the elliptic Hamiltonian constraint equation is solved on each time step to find $\phi$ while $\eta$, $K^r{}_r$, $K^\varphi{}_\varphi$, and $K^r{}_\theta$ are evolved.

A multigrid algorithm [15] is used to solve the quasilinear Hamiltonian constraint and linear maximal slicing equations. Fourier decomposition is used to solve the shift equations. Most results shown here were computed with a resolution of 290 radial and 18 angular zones. One quadrant (90°) in $\theta$ is modeled since equatorial plane symmetry is assumed. A rough parameter survey used a resolution of 180×18. Test calculations with higher angular resolutions show that quadrupole waves are adequately modeled with 18 angular zones (evenly spaced in angle).

Teukolsky [16] has described a quadrupole ($l=2$) order solution to the vacuum wave equation of linearized gravity in transverse-traceless gauge that can represent an arbitrary wave form. Abrahams and Evans [14] have expressed the $l=2$ solution in quasi-isotropic gauge and found solutions for other multipole orders. These solutions have been used as code tests [9,17], in investigations of wave-wave interactions [18], and as the basis for radiation extraction techniques [14,19,11]. To establish initial data for the present application where the fields are not arbitrarily weak, we first use an analytic expression for a linear ingoing quadrupolar wave to fix the freely specifiable parts of the metric and extrinsic curvature and then solve the constraint equations.

The quadrupole solution requires specification [16] of the quadrupole moment $I(v)$, its derivatives $I^{(1)}(v)\equiv dI(v)/dv$ and $I^{(2)}(v)$, and the integrals $I^{(-1)}(v)\equiv\int^v dv' I(v')$ and $I^{(-2)}(v)$. (Asymptotically, $h_+\to I^{(2)}\sin^2\theta/r$.) Here the advanced time is $v=t+r-r_0$ and the wave is centered at $r=r_0$ (chosen so that the gravitational field is initially weak, i.e., $r_0\gg M_p$, where $M_p$ is the packet mass) at $t=0$. We adopt a wave packet defined by $I^{(-2)}(v)=A\kappa\lambda^5[1-(v/\lambda)^2]^6$, where $A$ is the amplitude parameter, $\lambda$ is the width parameter, and $\kappa$ is a constant, $\kappa=\frac{1}{12288}\sqrt{143/\pi}$. The second derivative of the quadrupole moment is

$$I^{(2)}(v)=360A\kappa\lambda[1-20(v/\lambda)^2+70(v/\lambda)^4 -84(v/\lambda)^6+33(v/\lambda)^8],\quad |v|<\lambda\ , \quad (2)$$

which determines the profile of the asymptotic wave form. We take as the freely specifiable parts of the initial data the metric function $\eta$ and the extrinsic curvature component $K^r{}_\theta$ and fix them to have the form governed by the linear solution

$$\eta=\left[\frac{I^{(2)}(v)}{r}-2\frac{I^{(1)}(v)}{r^2}\right]\sin^2\theta\ , \quad (3)$$

and

$$\frac{K^r{}_\theta}{r}=2\left[\frac{I^{(2)}(v)}{r^2}-3\frac{I^{(1)}(v)}{r^3}+6\frac{I(v)}{r^4} -6\frac{I^{(-1)}(v)}{r^5}\right]\sin\theta\cos\theta\ . \quad (4)$$

The constraint equations then determine $\phi$, $K^r{}_r$, and $K^\varphi{}_\varphi$.

The wave form, shown in the inset of Fig. 1, has a characteristic wavelength $\simeq\lambda$. In the linear limit, the mass of the wave packet is

$$M_p^{\rm linear}=\frac{1}{2\pi}A^2\lambda\ . \quad (5)$$

For nearly linear initial data, the wave packet's Arnowitt-Deser-Misner (ADM) mass $M_p$ is typically $M_p<M_p^{\rm linear}$ by a fraction of $O(M_p/r_0)$.

A one-parameter sequence of gravitational wave implosions has been explored by varying the dimensionless amplitude $A$ or, equivalently, the strength parameter $\Theta\equiv 2\pi M_p/\lambda\simeq A^2$. Imploding waves with $\Theta\ll 1$ pass through themselves, only weakly self-interacting, and explode outward virtually unaffected. Stronger waves hold themselves together briefly as a geon [4], interacting nonlinearly, before exploding outward. For strength parameters sufficiently high ($\Theta\gtrsim\Theta_{\rm crit}\simeq 0.80$) the geon collapses and forms a black hole. Some portion of the wave-packet mass is trapped by the collapse while part of the wave escapes before the hole forms. Because the collapsing geon is asymmetrical, it initially forms a distorted black hole and some of the mass-energy emerges as quasi-normal-

mode (QNM) radiation as the black hole rings down.

When a black hole forms, the maximal time slices penetrate the horizon so that the hole's interior ends up being modeled in addition to the exterior. This leads to well-known problems in resolving the interior of the hole. Maximal time slices have been demonstrated to approach a limiting slice inside the horizon, with the obvious advantage that the domain of development avoids curvature singularities. A disadvantage is that a spatial coordinate singularity is asymptotically approached on the limiting time slice, which manifests itself as a throat inside the horizon of ever-increasing proper length [20]. Present schemes require that this throat region be resolved. The rapid lengthening of the throat produces sharp radial gradients in the fields and, without compensation, the simulations lose resolution and all accuracy within a time $\Delta t \sim 10 M_{\rm BH}$ of forming the hole. Compensation can be afforded by allowing radial mesh points to have time-dependent coordinate locations [8]. We use such a moving mesh algorithm to maintain resolution of the throat after a black hole forms. Radial mesh points are redistributed within a radius $r \lesssim 6.5 M_p$, preserving the original resolution of much of the exterior where gravitational radiation emerges.

The wave form is extracted by two separate means. The first computes and analyzes the Weyl scalar $\Psi_2$ while the second analyzes gauge-invariant variables constructed from the spatial metric (see Refs. [11,14] for details). Part of the process in each method involves removing the near-zone field to reveal the approximate asymptotic wave form. This process is essential, as wave forms must be read off close to the hole given the brief duration a simulation remains reliable once a hole forms. To check consistency, the two wave forms are compared to each other and to those extracted at other radii. While for $r_{\rm extract} \gg M_{\rm BH}$ we expect both methods to approximate well the asymptotic wave amplitude $h_+$, it appears feasible to obtain useful results at radii as small as $r_{\rm extract} \sim 8 M_{\rm BH}$ (used with the $\Psi_2$ method to obtain the wave form plotted in Fig. 3).

We have computed a spacetime that forms a black hole starting from an initial wave with $\Theta = 1.06 \simeq 1.3 \Theta_{\rm crit}$. Using the moving radial mesh faithful results were maintained for a time $\simeq 40 M_{\rm BH}$ after black hole formation.

Figure 1 shows the central value of the lapse function, $\alpha_c$ as a function of time as the wave implodes. Interestingly, the imploding wave causes $\alpha_c$ to oscillate several times before collapsing exponentially as the black hole forms. The exponential collapse proceeds with an $e$-folding time of about $t_e = 2.3 M_{\rm BH}$, distinct from the value $t_e = 1.80 M_{\rm BH}$ previously found for spherical dust collapse on maximal slices [21]. For comparison, Fig. 1 also displays $\alpha_c$ versus time for a spacetime containing a weaker wave, $\Theta \simeq 0.578$, that fails to form a hole. Similar oscillations occur, reaching $\alpha_c^{\rm min} \simeq 0.4$ before the wave emerges.

We searched for MOTS's in the spacetime using a shooting method [22]. As anticipated by previous studies (e.g., Ref. [20]) we locate both the outermost MOTS (the apparent horizon) and another inner one. In Fig. 2 the coordinate positions of these surfaces are superimposed

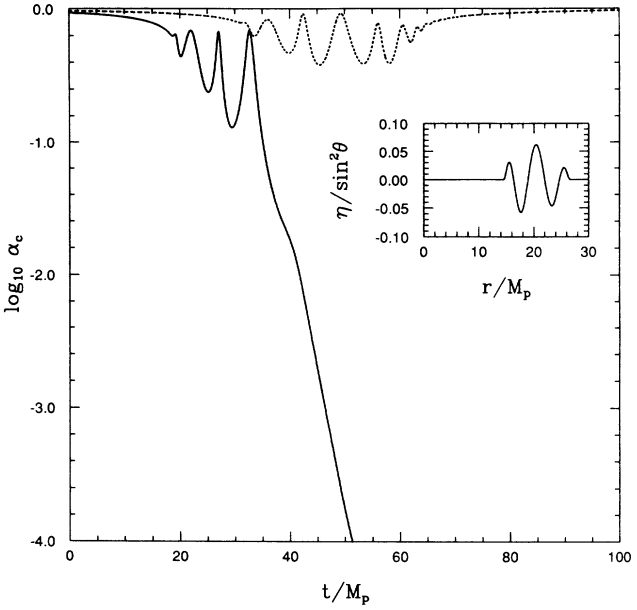


FIG. 1. Central value of the lapse function $\alpha_c$ for two imploding-wave spacetimes versus coordinate time (scaled to respective values of $M_p$). Cases shown are for strength parameters $\Theta = 1.06$ (solid curve) and $\Theta = 0.578$ (dashed curve). The latter wave, being weaker, implodes and then reemerges, taking the central lapse down to $\alpha_c^{\rm min} \simeq 0.4$. The solid curve depicts the strong oscillations in and subsequent exponential collapse of the lapse (with maximal time slicing) as the black hole forms. The inset shows the initial radial profile in $\eta$, and hence the shape of the wave packet, for this case. The radial scale of the wave form in the inset matches the temporal scale of the lapse plot, making evident the effect of the radial structure of the wave packet on $\alpha_c$.

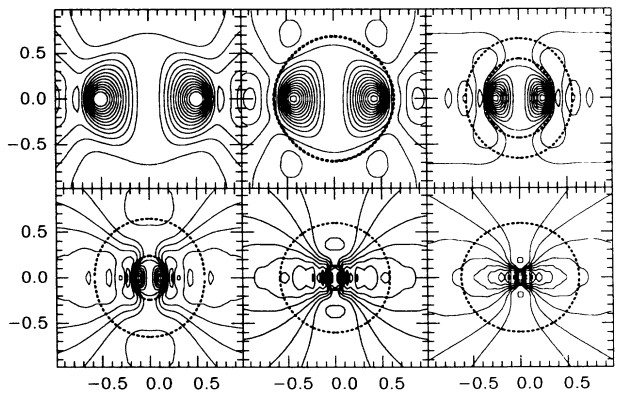


FIG. 2. Locations and evolution of marginally outer-trapped surfaces that arise as the imploding wave forms a black hole. Marginally outer-trapped surfaces are depicted by dashed curves. Contours of the radiative variable $\eta$ are shown, linearly spaced between values of $-0.9$ and 0.9. Coordinate radii are in units of the final black hole mass $M_{\rm BH}$. Coordinate times for the frames (read left to right, then top to bottom) are $t - t_{\rm BH} = -0.42 M_{\rm BH}$, $0.02 M_{\rm BH}$, $1.55 M_{\rm BH}$, $2.82 M_{\rm BH}$, $4.18 M_{\rm BH}$, and $5.63 M_{\rm BH}$.

on contours of the radiative variable $\eta$. When the black hole first forms (at $t=37.1M_p$), these two surfaces coincide. As the black hole evolves, the inner surface shrinks as the region of trapped surfaces engulfs the interior while the apparent horizon grows until it coincides with the event horizon. In Oppenheimer-Snyder dust collapse the inner MOTS reaches zero radius at the singularity. With maximal slicing, the time slices limit well away from the singularity causing the proper location of the inner MOTS to freeze. We observe a similar effect in this new spacetime, with the area of the inner MOTS freezing at a value corresponding to a mass of $0.76M_{\rm BH}$ (within a time $\Delta t \simeq 10M_p$). Note in Fig. 2 that this surface *appears* to shrink to $r=0$. This is evidence of quasi-isotropic spatial gauge giving rise to an impending spatial coordinate singularity as the limit slice is approached, causing the coordinate radii of the inner edge of the throat and all points interior to vanish exponentially.

The mass of the apparent horizon (computed from its area as $\sqrt{\mathcal{A}_{\rm AH}/16\pi}$), when it first appears, is $M_{\rm AH}=0.9M_{\rm BH}$, but climbs to within 4% of its ultimate mass in a time of about $3M_p$ and within 1% after $10M_p$. Ultimately, in the case reported here, the mass of the apparent horizon reaches $M_{\rm BH}\simeq 0.90M_p$. A recent study of massless scalar field collapse in spherical symmetry [23] has shown that a black hole with an arbitrarily small mass, compared to the mass of the wave packet, may be formed from a wave packet whose amplitude, or other parameter $p$, is sufficiently close to a critical value. A power-law relation has been discovered between the black hole mass and the critical parameter separation of the form $M_{\rm BH}\sim C|p-p_{\rm crit}|^{\beta}$, an apparent example of *critical phenomena*. In another paper [24] we address the issue of critical behavior in axisymmetric gravitational radiation collapse.

In Fig. 2 we also observe how coordinate radius distortions of the apparent horizon evolve as the black hole rings down. The apparent horizon is prolate when it first forms but by a time of about $4M_{\rm BH}$ later is spherical and by the final frame of Fig. 2 is oblate. The time scale of this oscillation is consistent with the period of the lowest $l=2$ QNM. A similar oscillation occurs in the ratio of polar-to-equatorial apparent horizon circumferences.

The outgoing quadrupole radiation emerging from the black hole is extracted using the methods previously described. Shortly after the apparent horizon first appears the wave form is dominated by QNM radiation (see Fig. 3). A least-squares fit is made of the wave form with the two most slowly damped quadrupole Schwarzschild QNM's ($\omega_1=(0.373\,67+0.088\,96i)\times M_{\rm BH}^{-1}$ and $\omega_2=(0.348\,44+0.274\,69i)\times M_{\rm BH}^{-1}$ [25]). The fit is made between the times $u=3M_{\rm BH}$ and $u=45M_{\rm BH}$. The time $u=0$ corresponds roughly to when the black hole's formation is causally apparent at the wave extraction radius. Prior to $u=0$ a remnant of the original wave packet escapes ahead of the forming black hole. Near $u=0$ the black hole's mass is still increasing and the wave form is not yet accurately given by the QNM fit. After $u\simeq 3M_{\rm BH}$ the QNM fit represents the wave form to about 1% (with an $L_2$ norm of $2.9\times10^{-3}$ computed over the following two oscillations). Despite having been formed entirely from a quadrupole wave, the black hole's initial distortion is small; the total energy in outgoing QNM radiation is just over 2% of the black hole mass.

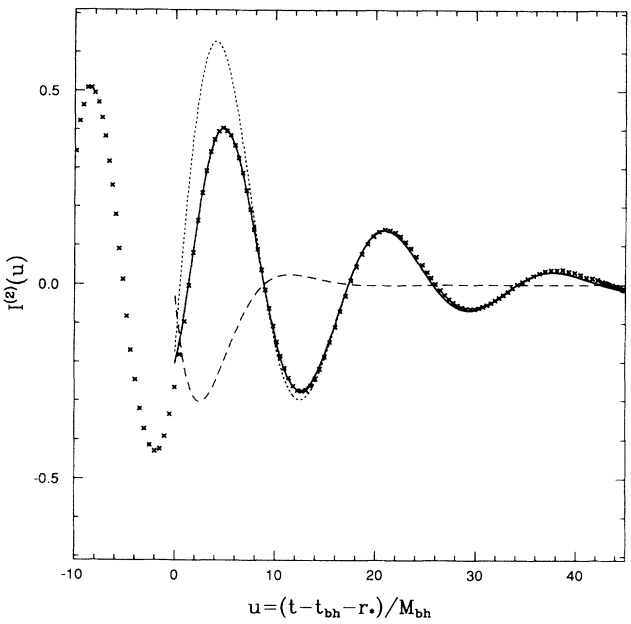


FIG. 3. Gravitational radiation ($l=2$) wave form emitted following black hole formation and normal mode fit. The extracted radiation signal (crosses) is shown plotted along with a fit (solid curve) of the signal using the two lowest-order Schwarzschild $l=2$ normal modes. The wave form is plotted versus retarded time relative to the epoch of black hole formation. Dotted and dashed curves show the two normal modes that comprise the fit of the wave form.

Using the $\Psi_2$ radiation extraction procedure mentioned above, we can also compute the $l=4$ outgoing radiation wave form. A least-squares fit analogous to that performed for $l=2$ again finds excellent agreement between this radiation and a superposition of Schwarzschild QNM's—in this case the three most slowly damped $l=4$ QNM's. By varying the mass and searching for the fit to the wave form that minimizes the $L_2$ norm, we have an independent estimate of the black hole mass. The mass we obtain from this method is consistent with the mass computed from the area of the apparent horizon at a level of 1%.

We thank G. Cook, A. Mezzacappa, L. Smarr, and K. Thorne for discussions. We are indebted to G. Cook for making available his black-box multigrid software. This research was supported in part by NSF Grants Nos. AST 90-15451 at Cornell University and PHY 90-01645 and PHY 90-57865 at the University of North Carolina. A.M.A. gratefully acknowledges the support of the NSF Division of Advanced Scientific Computing. C.R.E. thanks the Sloan Foundation for research support. Computations were performed at the North Carolina Supercomputing Center and at the NSF National Center for Supercomputing Applications.

[1] R. Beig and N. Ó Murchadha, Phys. Rev. Lett. **66**, 2421 (1991).

[2] See, for a summary, S. W. Hawking and G. F. R. Ellis, *The Large Scale Structure of Space-time* (Cambridge University Press, Cambridge, England, 1973).

[3] A. M. Abrahams, K. R. Heiderich, S. L. Shapiro, and S. A. Teukolsky, Phys. Rev. D **46**, 2452 (1992).

[4] See e.g., J. A. Wheeler, in *Relativity, Groups, and Topology,* edited by B. DeWitt and C. DeWitt (Gordon and Breach, New York, 1963); J. A. Wheeler, in *Geometrodynamics* (Academic, New York, 1962); R. Ruffini and J. A. Wheeler, Bull. Am. Phys. Soc. **15**, 76 (1970); C. W. Misner, K. S. Thorne, and J. A. Wheeler, *Gravitation* (Freeman, San Francisco, 1973), Sec. 35.8, p. 957.

[5] S. M. Miyama, Prog. Theor. Phys. **65**, 894 (1981).

[6] R. F. Stark and T. Piran, Phys. Rev. Lett. **55**, 891 (1985).

[7] S. L. Shapiro and S. A. Teukolsky, Phys. Rev. Lett. **66**, 994 (1991).

[8] C. R. Evans, Ph.D. thesis, University of Texas at Austin, 1984.

[9] C. R. Evans, in *Dynamical Spacetimes and Numerical Relativity,* edited by J. Centrella (Cambridge University Press, Cambridge, England, 1986).

[10] C. Evans, L. Smarr, and J. Wilson, in *Astrophysical Radiation Hydrodynamics,* edited by M. L. Norman and K.-H. A. Winkler (Reidel, Dordrecht, 1986).

[11] A. M. Abrahams and C. R. Evans, Phys. Rev. D **42**, 2585 (1990).

[12] A. M. Abrahams and C. R. Evans, in *Sixth Marcel Grossman Meeting on General Relativity,* Proceedings, Kyoto, Japan, 1991, edited by H. Sato (World Scientific, Singapore, 1992).

[13] J. M. Bardeen and T. Piran, Phys. Rep. **96**, 205 (1983).

[14] A. M. Abrahams and C. R. Evans, Phys. Rev. D **37**, 318 (1988).

[15] G. B. Cook, Phys. Rev. D **44**, 2293 (1991).

[16] S. A. Teukolsky, Phys. Rev. D **26**, 745 (1982).

[17] S. L. Shapiro and S. A. Teukolsky, Am. Sci. **79**, 330 (1991); T. Piran and R. F. Stark, in *Dynamical Spacetimes and Numerical Relativity* [9].

[18] A. M. Abrahams, Ph.D. thesis, University of Illinois at Urbana-Champaign, 1988.

[19] A. M. Abrahams, in *Frontiers in Numerical Relativity,* edited by C. R. Evans, L. S. Finn, and D. W. Hobill (Cambridge University Press, Cambridge, England, 1989), p. 110.

[20] D. M. Eardley and L. Smarr, Phys. Rev. D **19**, 2239 (1979).

[21] L. Smarr and J. W. York Jr., Phys. Rev. D **17**, 2529 (1978).

[22] P. G. Dykema, Ph.D. thesis, University of Texas at Austin, 1980.

[23] M. W. Choptuik, in *Approaches to Numerical Relativity,* edited by R. d'Inverno (Cambridge University Press, Cambridge, England, 1992).

[24] A. M. Abrahams and C. R. Evans (in preparation).

[25] S. Chandrasekhar and S. Detweiler, Proc. R. Soc. London **A344**, 441 (1975).